INTERNATIONAL JOURNAL OF CLIMATOLOGY
Int. J. Climatol. **37**: 443–454 (2017)
Published online 24 April 2016 in Wiley Online Library
(wileyonlinelibrary.com) DOI: 10.1002/joc.4717

RMetS
Royal Meteorological Society

A diagnostic equation for the daily maximum urban heat island effect for cities in northwestern Europe

Natalie E. Theeuwes,* Gert-Jan Steeneveld, Reinder J. Ronda and Albert A. M. Holtslag

Meteorology and Air Quality Section, Wageningen University, The Netherlands

ABSTRACT: The urban heat island (UHI) effect, defined as the air temperature difference between the urban canyon and the nearby rural area, is investigated. Because not all cities around the world are equipped with an extensive measurement network, a need exists for a relatively straightforward equation for the UHI effect. Here, we derive a simple, diagnostic equation for the UHI using dimensional analysis. This equation provides a first-order estimation of the daily maximum UHI based on routine meteorological observations and straightforward urban morphological properties. The equation is tested for 14 cities across northwestern Europe and appears to be robust. The comprehensiveness of this analytical equation allows for applications beyond urban meteorological studies.

KEY WORDS urban heat island; urban climate; meteorological observations; Western Europe; dimensional analysis; Buckingham-Π

Received 9 October 2015; Revised 22 January 2016; Accepted 19 February 2016

1. Introduction

The best known phenomenon resulting from the difference in urban and rural microclimates is the urban heat island effect (UHI). Here, the UHI is defined as the difference in air temperature between the urban street canyon and the rural environment, and is largest during the evening and night-time, typically in the order of ∼6 K during calm, fair weather conditions in northwestern Europe (Steeneveld *et al.*, 2011). In general, the UHI is induced by energy balance differences between land use types (Oke, 1982). Urban areas as a whole have a relatively low albedo and a relatively large heat storage in the urban fabric during daytime and subsequent release during the night. The released energy via thermal radiation is generally efficiently trapped in the urban canyons. In addition, extra heat release as a result of human activities and less evapotranspiration due to the lack of vegetation compared to the rural surroundings all lead to higher temperatures in urban areas. Consequently, the UHI generally depends on urban characteristics, such as street geometry and urban vegetation fraction.

Apart from the urban morphological properties, the location and climate of the city surroundings and meteorological conditions play important roles in determining the UHI magnitude as well. Because of the myriad of processes governing the urban climate, there have been only a few attempts to find a diagnostic equation to estimate the UHI within the urban canopy (Arnfield, 2003). However, research and operational activities in urban design, health studies and energy demand planning may benefit from reliable UHI estimates using these types of straightforward equations.

The UHI undergoes a diurnal cycle (Oke, 1982); during the morning and early-afternoon, the UHI is smallest and can become negative in some cases (Morris *et al.*, 2001; Theeuwes *et al.*, 2015). However, at the end of the afternoon, the incoming solar radiation decreases and both the urban and the rural environments cool. The urban area retains more heat and cools slower than the rural surroundings, causing the UHI to reach a maximum during the evening or night.

The maximum observed UHI ($UHI_{\max} = \max(T_{\text{urban}} - T_{\text{rural}})$) has been positively (and occasionally negatively) related to the aspect ratio or sky-view factor (e.g. Oke, 1981; Eliasson, 1996; Marciotto *et al.*, 2010; Theeuwes *et al.*, 2014), negatively related to vegetation (e.g. Dimoudi and Nikolopoulou, 2003; Steeneveld *et al.*, 2011; Petralli *et al.*, 2014) and negatively related to cloud cover and wind speed (i.e. Ackerman, 1985; Kidder and Essenwanger, 1995; Morris *et al.*, 2001). Nowadays, the UHI is often successfully modelled with sophisticated atmospheric mesoscale models coupled to an urban canopy or building energy model (e.g. Chen *et al.*, 2011; Salamanca *et al.*, 2011; Kusaka *et al.*, 2012). However, these models still take a substantial amount of computing time and are not easy to use for non-experts. In addition, they require a large amount of input parameters and initialisation data that are often not available or uncertain. Alternatively, statistical models have been utilized, usually linear regression (i.e. Bottyán and Unger, 2003; Hoffmann *et al.*, 2012; Szymanowski and Kryza, 2012). These methods are relatively

* Correspondence to: N. E. Theeuwes, Meteorology and Air Quality Section, Wageningen University, P.O. Box 47, 6700 AA Wageningen, The Netherlands. E-mail: Natalie.Theeuwes@wur.nl

straightforward and easy to use, but not purely physically based and require retuning for each city.

Alternatively, in this research, we present a physically based equation to diagnose a typical UHI_{max} at street level for various urban locations and weather types in northwestern Europe. A novel aspect of our approach is the application of the well-established method of dimensional analysis (Buckingham, 1914; Langhaar, 1951) for the application in urban meteorology. Previous scaling approaches have been attempted by Summers (1964), Oke and East (1971), Oke (1998), Hidalgo *et al.* (2010), and Lee *et al.* (2014). Most of these scalings are based on variables that are relatively difficult to measure, such as the boundary-layer height and the surface sensible heat flux in urban and rural locations, thus are difficult to apply to most cities.

The diagnostic equation of this study is based on routine, rural weather observations and basic city characteristics that should be easily accessible (Section 2). An analysis to identify the meteorological variables essential for the estimation of the UHI_{max} similar to Oke (1998) is given in Section 3. The diagnostic equation is derived (Section 4) and subsequently evaluated (Section 5) with observations from other weather stations from hobby meteorologists in northwestern Europe and for a wide range of city sizes (Section 6). The final goal is to provide non-experts with a tool to make a first-order estimate of UHI_{max}.

2. Observations

Routine temperature measurements in urban areas are still scarce, because the complex terrain causes issues concerning representativeness, maintenance and vandalism. However, many hobby meteorologists measure temperatures within cities. These observations have been used before to analyse the UHI in various cities in the Netherlands by Steeneveld *et al.* (2011) and Wolters and Brandsma (2012). These have been found to be very valuable after careful screening. In order to quantify the extremity of the observations of UHI_{max}, the observations were fit through a generalized extreme value distribution (GEV) as in Steeneveld *et al.* (2011). Stations for which the data showed a large deviation from the GEV curve were not used in the analysis. Deviation from the GEV curve might mean that the weather station has been moved or been indoors for a period of time.

Here, we use 11 hobby meteorology stations across northwestern Europe to derive and evaluate the equation for the UHI_{max} (Table 1). These stations have been selected for a measurement height of around 1.50 m above the surface; no roof stations were considered. Most of these stations are Davis Vantage pro 2 stations with active 24-h ventilation and have a very low bias (0.2 K) according to Bell *et al.* (2015). The Alecto stations also have active ventilation, whereas the Cresta and La Crosse stations are naturally ventilated.

Two additional stations are located in Wageningen and in Amsterdam, and consist of Davis solar powered, ventilated

Table 1. Characteristics of the urban measurement stations used.

Abr.	City	Rural station	Instrumentation	Coordinates	Distance from rural station, km	LCZ	Vegetation fraction	SVF	Inhabitants	Time
P1	Paris	Grignon	Davis Vantage Pro	48.852°N, 2.336°E	28.5	2	0.05	0.23	2.25×10^6	1/2006–12/2008
A	Amsterdam	Schiphol	Davis screen & Decagon VP-30	52.351°N, 4.894°E	11.8	2	0.08	0.39	8.23×10^5	5/2014–2/2015
L	London	Kenley	Davis Vantage Pro	51.524°N, −0.134°E	24.5	2	0.14	0.27	8.42×10^6	1/2012–7/2015
K	Köln	Jülich	Davis Vantage Vue	50.931°N, 6.959°E	37.3	2/5	0.04	0.68	1.03×10^6	2/2013–12/2014
O	Oss	Volkel	Davis Vantage Pro 2	51.762°N, 5.513°E	18.1	3	0.19	0.53	5.75×10^4	1/2014–12/2014
N	Nijmegen	Volkel	Davis Vantage Pro 2	51.837°N, 5.839°E	23.0	3	0.20	0.52	1.69×10^5	8/2010–12/2014
W	Wageningen	Veenkampen	Davis screen & Decagon VP-30	51.974°N, 5.671°E	3.7	3	0.21	0.57	3.74×10^4	5/2013–5/2014
H1	Hoogeveen	Hoogeveen	Davis Vantage Pro 2	52.724°N, 6.516°E	4.2	3	0.36	0.72	3.89×10^4	2/2011–1/2015
T	Tilburg	Gilze-Rijen	Cresta WXR815LM	51.553°N, 5.095°E	11.6	3	0.37	0.60	1.91×10^5	8/2009–1/2015
U	Utrecht	De Bilt	Alecto WS-4000	52.079°N, 5.139°E	3.7	3	0.38	0.61	3.31×10^5	3/2009–3/2015
B	Birmingham	Coleshill	Vaisala WXT520	52.472°N, −1.901°E	10.3	5	0.27	0.84	1.09×10^6	1/2014–12/2014
P2	Palaiseau	Grignon	La Crosse WS-2305	48.724°N, 2.251°E	25.9	5/6	0.29	0.66	3.03×10^4	6/2005–12/2008
H2	Hoogezand	Eelde	Davis Vantage Pro 2	53.159°N, 6.759°E	12.5	6	0.30	0.70	2.14×10^4	4/2012–3/2015
G	Groningen	Eelde	Davis Vantage Pro 2	53.232°N, 6.604°E	12.0	6	0.39	0.66	1.98×10^5	12/2012–3/2015

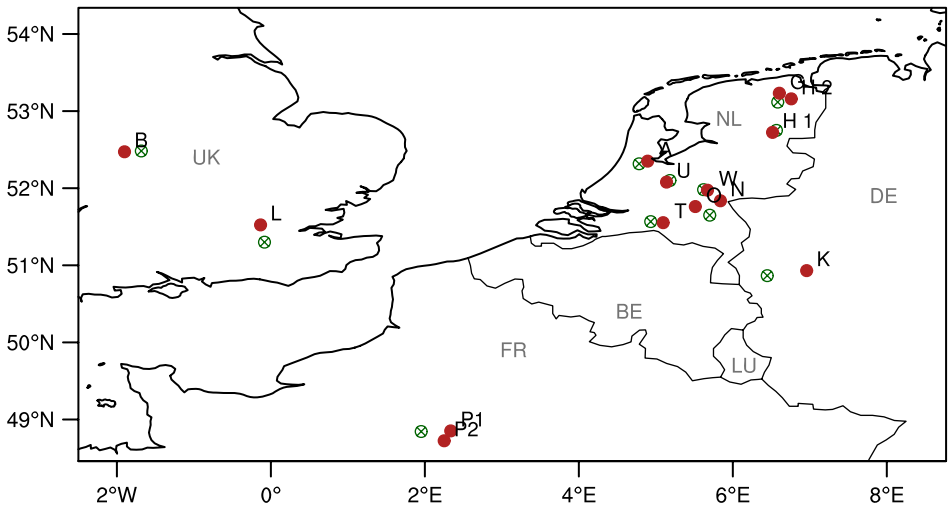

Figure 1. The locations of the different measurement stations, the red, closed dots indicate measurement stations in urban areas and the green, crossed dots in rural areas. The abbreviations of the city names can be found in Table 1. Abbreviations for the countries are shown in grey.

radiation screens, and Decagon VP-30 temperature and humidity sensors with a Decagon EM50G logger. Note that the screens are the same as those of the Davis Vantage Pro 2 weather station, but are only ventilated when the solar panels receive direct incoming radiation. The construction consists of an east facing and a westward facing solar panel, specially designed to collect inside the urban canyon. These stations have been attached to lampposts at a height of 3 m in Wageningen and 4 m in Amsterdam.

Finally, the weather station set-up in Birmingham is a Vaisala WXT520 weather transmitter sampling every 15 s using SDI-12 protocol logging 1-min averages. The measurement height is around 3 m above the surface. For more information about the Birmingham measurement network, see Chapman *et al.* (2015).

Table 1 summarizes the characteristics of each urban station. The vegetation fraction within a 500-m radius of the urban weather stations vary, but is below 0.40 for all stations. The local climate zones (LCZ; Stewart and Oke, 2012) are mostly compact and open mid- and low-rise. Finally, the sky view factor (SVF) varies between 0.23 and 0.84.

In order to compute an $UHI_{\max}$ and quantify the meteorological variables, observations from rural areas surrounding the city are also needed. Therefore, observations of temperature, wind, solar radiation, rain and relative humidity in the Netherlands are provided by the Dutch National Weather Service and the United Kingdom Met Office (Figure 1). These measurement stations are located at airports (except Hoogeveen and De Bilt) over a grass surface (LCZ D, low plants), in accordance with World Meteorological Organization (WMO) standards. Data from Wageningen were compared to the meteorological station 'Veenkampen' (51.981°N, 5.622°E) maintained by Wageningen University and also located over grass surface. For the cities in France and Germany, data from the European Fluxes Database Cluster are used. The rural reference station of Köln was located near Jülich above cropland. A flux station near Grignon was used for computing the UHI in Paris and Palaiseau (Figure 1). This station was also located over a crop surface and was used previously by Lehuger *et al.* (2010).

For the analysis, some weather phenomena need to be accounted for. These events can cause differences in the urban and rural temperatures not related to the UHI (Fortuniak *et al.*, 2006). In order to exclude frontal systems, rain events (daily sum > 0.3 mm) and sudden changes in the wind speed (wind speed changes >2 ms^{-1} per hour) have been excluded. Finally, for fog events, days with averaged relative humidity $> 80\%$ have been excluded. Excluding these days leaves between 25 and 40% of the data for further analysis. While performing the dimensional analysis, heating degree days of more than 17 have been excluded (base temperature is 18 °C) in order to exclude the largest anthropogenic heat fluxes.

3. Selecting variables

For designing a diagnostic equation of the $UHI_{\max}$, it is essential to select the variables that impact the $UHI_{\max}$ most and are physically based. The rural temperature is mainly dependent on weather conditions; night-time cooling is determined by wind and cloud cover with maximum cooling under low winds and clear skies. In addition, we may expect that the $UHI_{\max}$ depends on the energy stored in the urban canopy during daytime by solar radiation. As such, we can postulate the following variables (Table 2) (urban-related variables will be introduced later):

- $S^{\downarrow}$ [K ms^{-1}]: the incoming shortwave radiation as averaged over the day at the rural site, to indicate the energy entering the system (e.g. Ackerman, 1985; Kidder and Essenwanger, 1995; Morris *et al.*, 2001). We express $S^{\downarrow}$ in kinematic units [K ms^{-1}], so the amount of incoming radiation in Wm^{-2} divided by the air density and specific heat capacity (ρC_p)

Table 2. Information about the selected variables for the analysis.

Variable	Time (local time)	Description
UHI_{max}	Day 0, 0800–day 1, 0700	$\max(T_{urban} - T_{rural})$ from 1-h average data
$S^{\downarrow}$	Day 0, 0100–day 1, 0000	Sum of the shortwave incoming radiation from 1-h maxima in rural area divided by 24 h
U	Day 0, 0800–day 1, 0700	Average wind speed at 10 m from 1-h averages in rural area
D_{avg}	Day 0, 0800–day 1, 0700	Average wind direction at 10 m from 1-h averages in rural area
DTR	Day 0, 0800–day 1, 0700	Difference between the maximum and minimum temperature in rural area
$\frac{\Delta T}{\Delta z}$	Day 0, 1700–day 1, 0700	$\frac{\min(T_{1.5m}) - \min(T_{10cm})}{1.5-0.1}$ Difference between the minimum rural temperature at 1.5 m and at 10 cm in rural area
R_{sum}	Day 0, 0100–day 1, 000	The total sum of rain from one-h averages in rural area

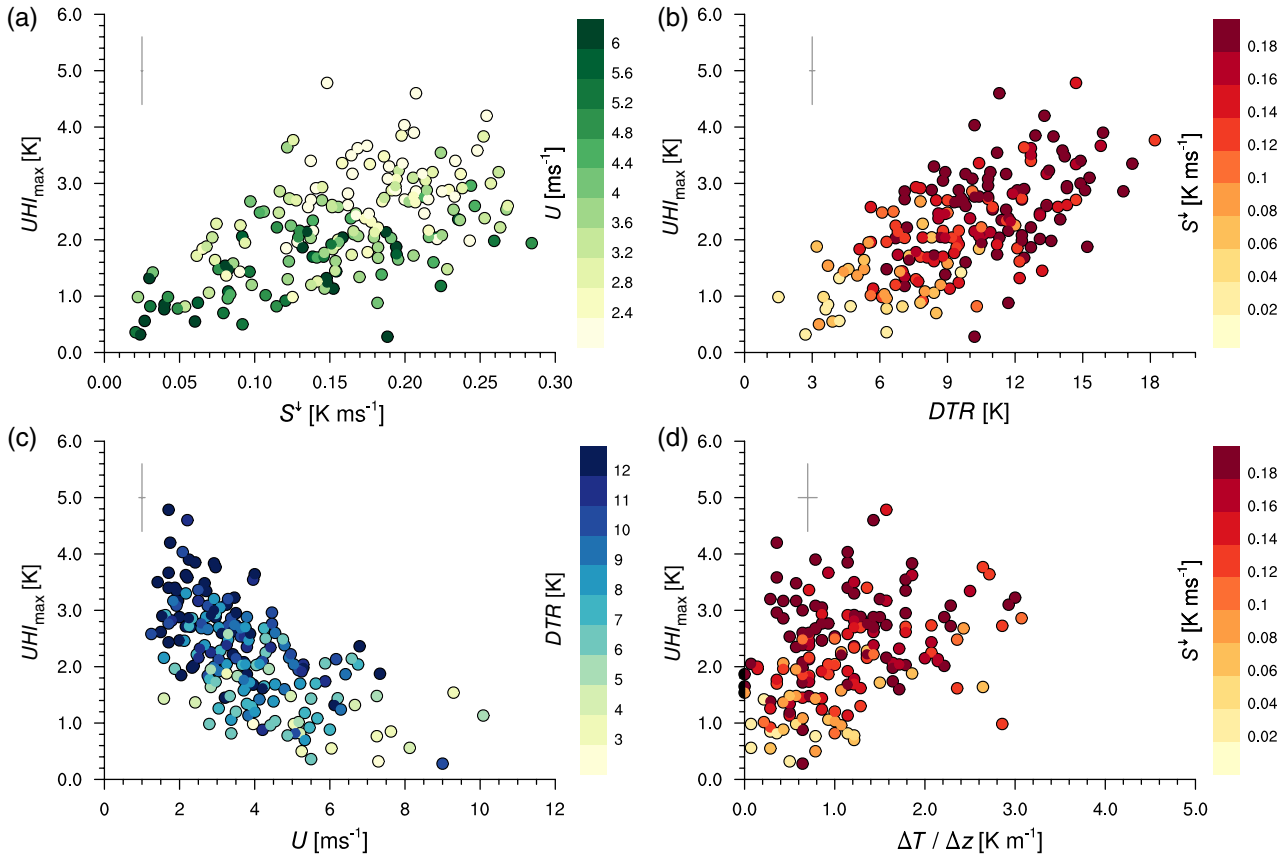

Figure 2. The observed UHI_{max} against (a) the diurnally averaged incoming shortwave radiation, (b) the diurnal temperature range, (c) the diurnally averaged wind speed at 10 m and (d) the temperature gradient close to the ground, all at the rural location, for the station in Hoogeveen. The colours indicate the magnitude of other variables, green in (a) is the wind speed, red in (b) and (d) is the incoming shortwave radiation and blue in (c) is the diurnal temperature range. The grey lines in the upper-left corner indicate the measurement error based on the instrument uncertainty. The data with rain ($R_{sum} > 0.3$ mm) and fog (relative humidity > 80%) have been excluded.

- DTR [K]: the diurnal temperature range at the rural site ($T_{max} - T_{min}$), to introduce a measure for the cooling potential during the night outside the city (e.g. Gallo *et al.*, 1996; Holmer *et al.*, 2013). A higher diurnal temperature range indicates that lower night-time temperatures can be reached at the rural site and thus a higher UHI_{max}.
- U_{avg} [ms^{-1}]: the 24 h average 10-m wind speed during the day and night at the rural site (e.g. Ackerman, 1985; Kidder and Essenwanger, 1995; Morris *et al.*, 2001). A stronger wind speed will mix horizontal and vertical temperature differences more effectively and will decrease the UHI_{max}.
- $\frac{\Delta T}{\Delta z}$ [K m^{-1}]: the maximum temperature gradient (in this study between 2 m and 10 cm) close to the ground at night at the rural site acts as a measure for stability during the night (e.g. Lee, 1979; Baik *et al.*, 2007; Hu *et al.*, 2013). This variable could be included as an alternative to the diurnal temperature range (DTR).

Figure 2 shows these four variables and their relation to the measured daily maximum UHI (UHI_{max}) for an urban

station (Hoogeveen). This location was selected because it is not located on the edge of the city and has very little influence of mesoscale flows, due to orography or proximity to the sea and ideally located to answer our research question.

As expected, the incoming shortwave radiation has a positive relation with the $UHI_{\max}$ (Figure 2(a)), consistent with Steeneveld *et al.* (2011). Note that $S^{\downarrow}$ is both influenced by clouds and the season since we analyse data at mid-latitude locations. An increase in the energy entering the urban canopy increases the heat that is released during the night from the urban fabric, elevating the temperature difference between the urban and rural environment. Generally, the difference in wind speed explains the large scatter in the relation between $S^{\downarrow}$ and $UHI_{\max}$.

As shown in Figure 2(b), the diurnal temperature range is positively correlated with $UHI_{\max}$. The *DTR* has been successfully related to the urban and rural cooling rate by Holmer *et al.* (2013). If the rural environment becomes more stable, the minimum temperature is able to reach a lower value and the *DTR* increases. The night-time urban temperature does not decrease as much as the rural temperature, causing a large $UHI_{\max}$ under stable conditions with a high *DTR*. Figure 2(b) also shows that the large *DTR* is also closely related to the incoming shortwave radiation. This can be explained, because during clear sky days, the maximum (and minimum) temperature can reach much higher (and lower) values than during cloudy days (and nights).

The wind speed appears to be negatively correlated with the $UHI_{\max}$ (Figure 2(c)), as many other studies have shown before (e.g. Ackerman, 1985; Park, 1986; Kidder and Essenwanger, 1995; Morris *et al.*, 2001). The increased wind speed leads to more mixing, both in the vertical and the horizontal direction. A higher wind speed leads to more vertical mixing and in the horizontal direction and a reduction in the stability of the rural environment. As the urban environment stays neutral or slightly unstable, an enhanced wind speed usually leads to a lower $UHI_{\max}$ as well. In addition, enhanced mixing between the rural and urban environment, local advection, reduces the $UHI_{\max}$. Overall, the figures indicate that both the wind speed and diurnal temperature range will need to be included in the equation.

Finally, we also explore the vertical temperature gradient $\frac{\Delta T}{\Delta z}$ in the rural area near the surface, which is another measure of the atmospheric stability in the rural environment. This variable is positively related to the $UHI_{\max}$ (Figure 2(d)). When near surface atmospheric stratification develops, turbulence is suppressed, decreasing the sensible heat flux, leading to a lower rural temperature (Steeneveld *et al.*, 2006). On the other hand, the air in urban areas mostly remains relatively well mixed, due to night-time heat release, thus limiting urban cooling. As a result, a more stable rural area increases the urban–rural temperature difference and $UHI_{\max}$. This variable is shown to be more independent of the shortwave incoming radiation, because the maximum temperature gradient is mainly governed by the nocturnal state of the atmosphere. The temperature gradient–$UHI_{\max}$ relation can be improved with the inclusion of incoming radiation, although the final result is not as evident compared to the DTR. Another disadvantage of $\frac{\Delta T}{\Delta z}$ is that it is not routinely observed outside of the Netherlands.

4. Designing equations

In this section, a diagnostic equation will be derived for the $UHI_{\max}$ from the meteorological variables described in the previous section. Therefore, the technique of dimensional analysis (Buckingham, 1914; Langhaar, 1951) is used, similar to the approach used by Steeneveld *et al.* (2007) and Hidalgo *et al.* (2010). Dimensional analysis is a method used to find a physically meaningful equation between variables based on their fundamental dimensions (e.g. time, length, mass). This technique has been proven to be very valuable in atmospheric sciences, for instance, Monin–Obukhov Similarity theory has provided the widely known flux profile relations that were developed using dimensional analysis (Businger *et al.*, 1971; Dyer, 1974).

Using Buckingham's Π theorem (Buckingham, 1914; Langhaar, 1951), dimensionless groups can be formulated with the variables as described above. For example, if only the variables $UHI_{\max}$, $S^{\downarrow}$, *DTR* and U are used, the following dimensionless groups can be constructed (see Appendix for the formal derivation):

$$\Pi_1 = \frac{UHI_{\max}}{DTR} \tag{1}$$

$$\Pi_2 = \frac{S^{\downarrow}}{U \cdot DTR} \tag{2}$$

Subsequently, a functional form between Π_1 and Π_2 is derived using observations, describing the relationship between these two groups. The two dimensionless groups are plotted as a function of each other in Figure 3(a). Note that Π_1 and Π_2 have the DTR as a common variable, this may lead to self-correlation (Baas *et al.*, 2006) and will be discussed in Section 7. The function that can be fit through the Hoogeveen data is:

$$\Pi_2 = c_1 \cdot \Pi_1^{\lambda} \tag{3}$$

Here, c_1 is a constant specific for the Hoogeveen data set and λ the exponent to be fit through the data. The equation can be rewritten as:

$$\frac{UHI_{\max}}{DTR} = a_1 \left(\frac{S^{\downarrow}}{U \cdot DTR} \right)^{\frac{1}{\lambda}} \tag{4}$$

Here, a_1 is a constant and a transformation of c_1: $a_1 = \sqrt[\lambda]{\frac{1}{c_1}}$. The constant a_1 relates to urban properties different for each city and surface properties differences within the city. In Section 6, a function for a_1 will be derived using urban properties important for cities in North Western Europe.

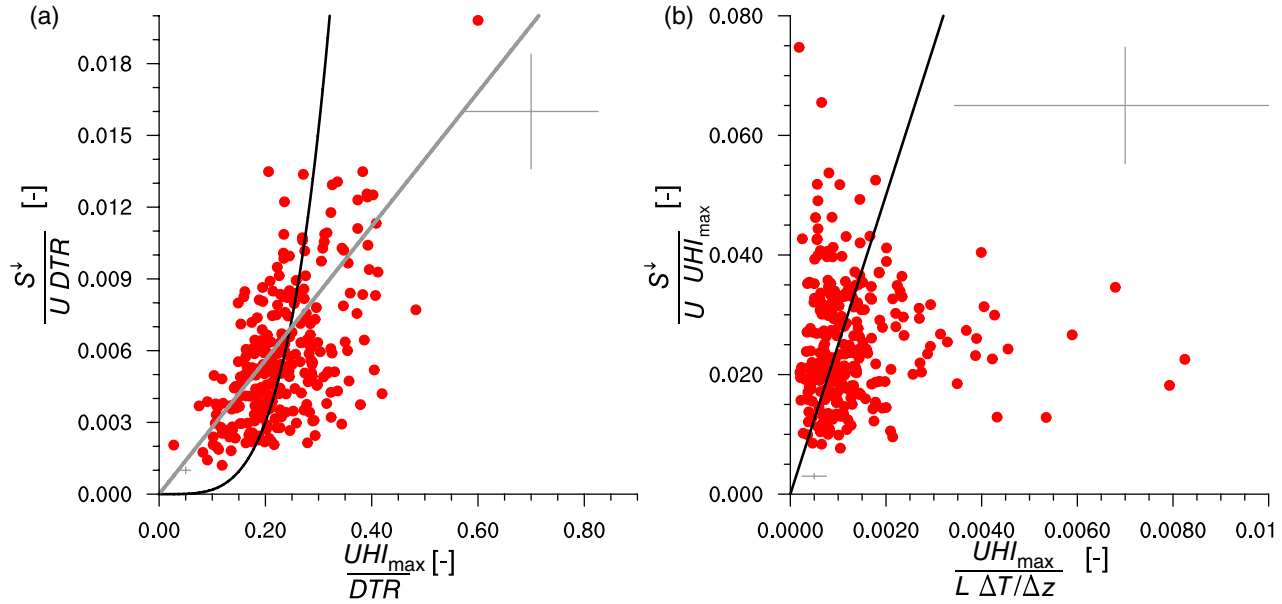

Figure 3. Two dimensionless groups plotted as a function of each other with data for the station in Hoogeveen. (a) Dimensionless groups derived in Equations (1) and (2) with trend lines of the functions $y = c_1 \cdot x^4$ (black) and $y = c_2 \cdot x$ (grey). (b) Dimensionless groups derived in Equations (8) and (9) with a trend line of the function $y = c_3 \cdot x$. The grey lines in the upper-right and lower-left corners indicate the measurement error based on the instrument uncertainty. The data with rain ($R_{sum} > 0.3$ mm), fog (relative humidity > 80%) and heating degree days higher than 17 have been excluded (base = 18 °C).

In Figure 3(a), two functions are shown and their fit through the Hoogeveen data, one with $\lambda = 4$ and one with $\lambda = 1$. Rewriting Equation (4) to make $UHI_{\max}$ explicit with $\lambda = 4$, we find:

$$UHI_{\max} = a_1 \sqrt[4]{\frac{S^{\downarrow} DTR^3}{U}} \tag{5}$$

On the other hand, rewriting Equation (4) for $UHI_{\max}$ with $\lambda = 1$ causes the DTR to cancel out and results in the following equation:

$$UHI_{\max} = \frac{a_2 S^{\downarrow}}{U} \tag{6}$$

Different values of λ have been tested. The λ with the lowest root mean squared error (RMSE) was 3.6, however the error for $\lambda = 4$ was only slightly larger; for $\lambda = 3.6$ the RMSE = 0.56 K compared to a RMSE = 0.63 for $\lambda = 4$.

In a similar manner, dimensional analysis can be performed with another combination of variables such as: $UHI_{\max}$, $S^{\downarrow}$, $\frac{\Delta T}{\Delta z}$, U and a length scale L. Then Buckingham's Π theorem states that two dimensionless groups can be formed, 5 variables − 3 dimensions [(K), (m) and (s)] = 2 groups.

Here, L (m) is chosen to be a horizontal length scale that could describe the distance of the city to a large water body and the distance from the station to the edge of the city. The location of the city with respect to the sea may be important to incorporate considering mesoscale effects bringing local advection of moisture and temperature into the city. These aspects are secondarily included in the DTR in Equation (5). In addition, the size of the city and the location of interest within the city are important to represent potential local advection and fetch length over the urban terrain. Therefore, a second length scale can be used to quantify the distance the wind travels over the city. The idea to formulate a length scale in this manner is widely used in the modelling of the nocturnal boundary layer (i.e. Blackadar, 1962; Delage, 1974), where the mixing length is formulated analogously, ensuring a smooth transition of the two length scales using inverse interpolation of the two individual length scales.

$$\frac{1}{L} = \frac{1}{L_{\text{cityedge}}} + \frac{1}{L_{\text{water}}} \tag{7}$$

In Equation (7), L_{cityedge} is the distance from the city measurement station to the edge of the city and L_{water} is the distance to a large water body, dependent on the wind direction. Therefore, as the wind direction changes, the distance to the edge of the city or to a large water body changes as well. A large water body has diameter larger than the distance from the shoreline to the urban weather station. Being close to the sea decreases L. For a location far inland, the last term in Equation (7) becomes negligible and only L_{cityedge} contributes, creating a physically realistic variable to be related to $UHI_{\max}$

Using these variables, the two following dimensionless groups can be formed:

$$\Pi_3 = \frac{UHI_{\max}}{\frac{\Delta T}{\Delta z} L}, \tag{8}$$

$$\Pi_4 = \frac{S^{\downarrow}}{\mathrm{U} \cdot UHI_{\max}} \tag{9}$$

The data for Hoogeveen shows that these two dimensionless group can be linearly related (Figure 3(b)):

$$\Pi_4 = c_3 \cdot \Pi_3 \tag{10}$$

Table 3. The best fit of constant a_i (based on the MEAE) fitted for one half of the data set and the root mean squared error and the median absolute error for the second half of the data set.

Equation	City	a_i best fit	RMSE (K)	MEAE (K)
5	Hoogeveen	0.97	0.75	0.52
5	Nijmegen	1.26	0.98	0.65
6	Hoogeveen	35.9	0.89	0.62
6	Nijmegen	51.5	1.61	1.08
11	Hoogeveen	0.20	0.82	0.54
11	Nijmegen	0.18	1.40	0.87

Rewriting this equation for $UHI_{\max}$ gives the following equation:

$$UHI_{\max} = a_3 \sqrt{\frac{S^{\downarrow} \frac{\Delta T}{\Delta z} L}{U}} \tag{11}$$

In Equations (5), (6) and (11), the a_i denote constants specific to each data set. Table 3 shows the best fit of a_i for each of the above mentioned equations. The data set was randomly split in two, i.e. a statistically independent calibration and validation data set. With this approach, we randomly exclude time-dependent errors (e.g. seasonality, minor changes in urban configuration and changes in vegetation). The values of a_i were determined with the calibration data set.

5. Evaluating the equations

Figure 4 shows the result of the three equations for the validation data set from two cities (Hoogeveen and Nijmegen). The trend lines show the best linear fit [based on the median absolute error (MEAE)] for a_i, and Table 3 shows the slope (a_i), the RMSE and MEAE for each of the equations.

Equation (5) shows a very close correspondence to the observed $UHI_{\max}$ (Figure 4(a)). For Hoogeveen, the relation performs slightly better than for Nijmegen, an RMSE of 0.75 K compared to an RMSE of 0.98 K. Given the instrument uncertainty displayed in the error bars, the difference in the RMSE is only minor. However, the overall performance of this equation is very good compared to the other two equations, that have RMSE's of 0.89 K *versus* 1.61 K and 0.82 K *versus* 1.40 K for Hoogeveen and Nijmegen.

Figure 4(b) displays the measured $UHI_{\max}$ with the result of Equation (6). When the $UHI_{\max}$ is higher than 3 K, it is increasingly underestimated, which seems to be caused by the wind speed. The key difference between this equation and Equations (5) and (11) is the relation between $UHI_{\max}$ and U is not a root function. Morris *et al.* (2001) found that the $UHI_{\max}$ could be best fitted with the fourth root function of U, as represented in Equation (5). In addition, the difference in the performance between Hoogeveen and Nijmegen is considerably large, RMSE = 0.89 K for Hoogeveen and 1.61 K for Nijmegen. This may indicate that in Nijmegen not all the relevant processes appear to be taken into account with this equation.

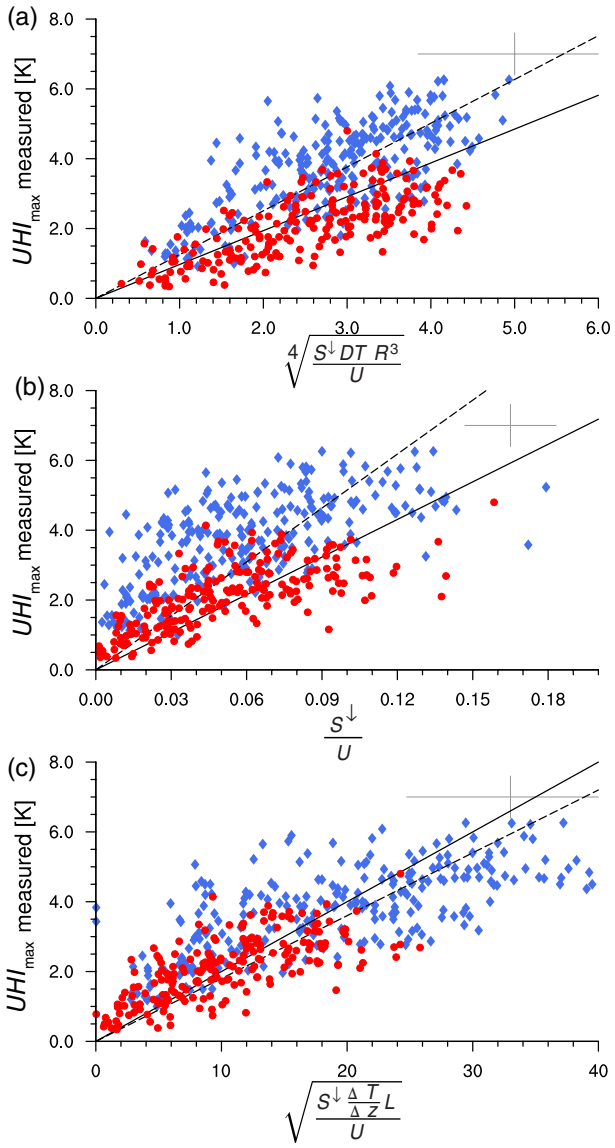

Figure 4. The observed $UHI_{\max}$ against the results from the three different equations: (a) Equation (5), (b) Equation (6) and (c) Equation (11). The red dots show data for the station in Hoogeveen and the blue diamonds for Nijmegen. The trend lines are given for the best fit for half of the data set of each station, solid lines are for Hoogeveen and dashed lines for Nijmegen. The RMSE and MEAE are given in Table 3. The grey lines in the upper-right corner indicate the measurement error based on the instrument uncertainty. The data with rain ($R_{sum} > 0.3$ mm) and fog (relative humidity > 80%) have been excluded.

As shown in Figure 4(c), model estimates with Equation (11) show a clear correlation with $UHI_{\max}$. In Hoogeveen, the equation again complies better with the observations than in Nijmegen, RMSE of 0.82 K *versus* 1.40 K. In both cities, the equation underestimates observed $UHI_{\max}$ lower than 3–4 K, and overestimates the UHI above 3–4 K. We clearly identify the effect of variable L in this equation. The constant a_3 that is best suited for the Nijmegen data ($a_3 = 0.18$) is close to the a_3 best fit for the Hoogeveen data ($a_3 = 0.20$).

Overall, Equation (5) best represents $UHI_{\max}$ for both Hoogeveen and Nijmegen. Therefore, in the remainder of this study, Equation (5) is used to estimate $UHI_{\max}$.

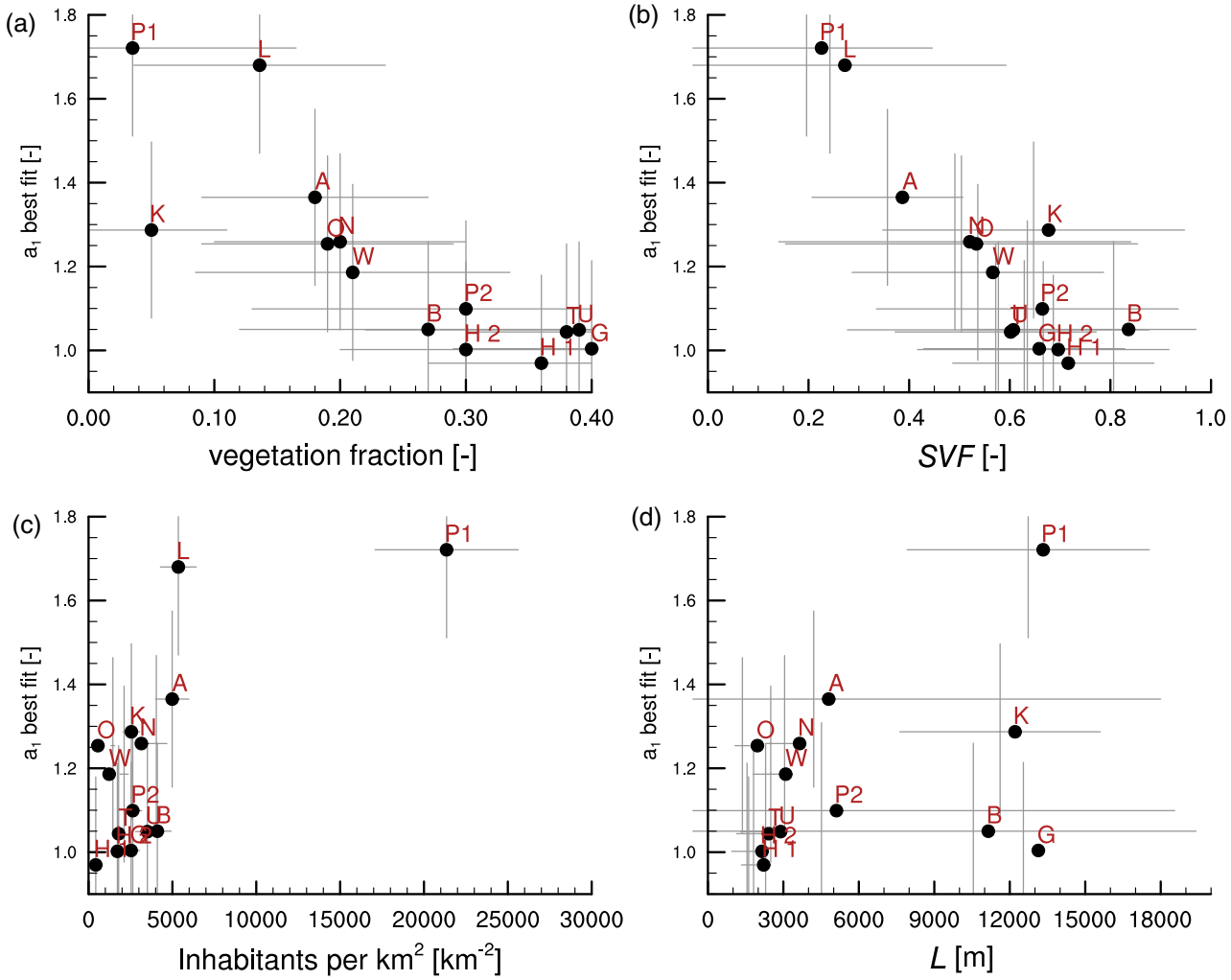

Figure 5. The best fit for a_1 for the first half of each of the city's data set against different urban characteristics: (a) vegetation fraction in a radius of 500 m around the urban measurement station, (b) sky-view factor, (c) population density of the city and (d) and the length scale from Equation (7). The abbreviations of the city names can be found in Table 1 and the grey lines indicate the error bars estimated from the uncertainty in the estimation of the urban properties and confidence in estimating a_1.

In order to make this equation applicable to other cities, we expect a_1 to be a function of urban morphological properties.

6. Application to other cities

The next step is to evaluate the performance of the diagnostic Equation (5) for other cities and to include urban morphological properties important for the estimation of the UHI_{max}. In order to quantify this effect, Figure 5 shows the dependence of a_1 in Equation (5) on various urban properties: the vegetation fraction in a radius of 500 m around the urban weather station, the sky-view factor at the stations location, estimated from the building heights and street width, the population density of the chosen city and the average horizontal length scale L (Section 4, Equation (7)).

Here, a_1 shows the best relation with the sky-view factor at the location of the station (Figure 5(b)). The vegetation fraction in a 500-m radius also shows a clear relationship with a_1 (Figure 5(a)), as well as the population density (Figure 5(c)), in line with previous research (e.g. Oke, 1981; Steeneveld *et al.*, 2011). However, the distribution of the population density is insufficient in order to concretely relate to a_1. The length scale L appears not to be convincingly related with a_1 and is not considered to be a meaningful parameter for further analysis. The relation between the UHI and vegetation fraction was tested for several radii, and 500 m showed the most convincing result.

Given the findings, we use the vegetation fraction and sky-view factor to represent a_1. Because both variables show a linear relation to a_1, a multiple linear regression method is applied to find the relation between the sky-view factor and vegetation and a_1. This results in an equation: $a_1 = 1.94 - 0.93 \cdot SVF - 0.88 \cdot f_{veg}$ that we simplify to (Figure (6)):

$$a_1 = 2 - SVF - f_{veg} \tag{12}$$

recognizing the large error bars in the coefficients. With this rounding-off approximation, the MEAE of a_1

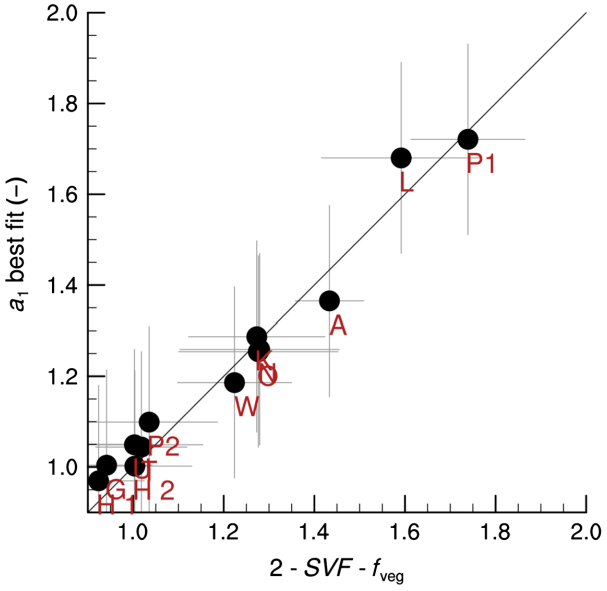

Figure 6. The best fit for a_1 for the first half of each of the city's data set against Equation (12). The solid line indicates the function $y = x$. The abbreviations of the city names can be found in Table 1 and the grey lines indicate the error bars estimated from the uncertainty in the estimation of the urban properties and confidence in estimating a_1.

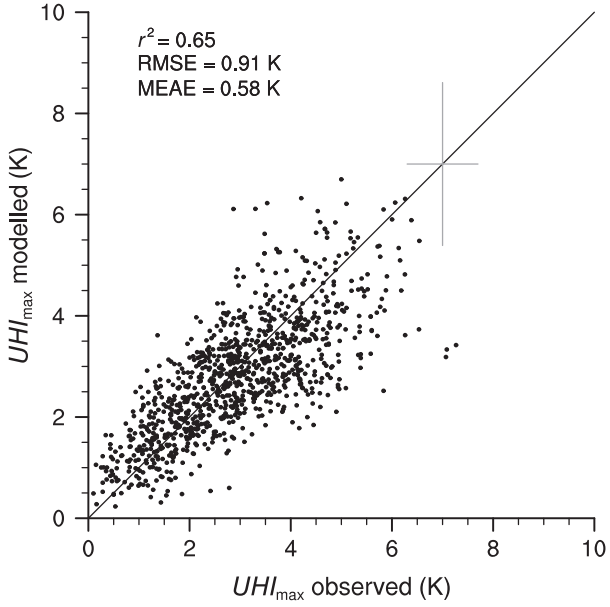

Figure 7. The observed UHI_{max} against the predicted UHI_{max} using Equation (13) for all stations. The solid line is the one-to-one line. The grey lines in the upper-right corner indicate the error bars estimated from the measurement (instrument) and model uncertainty. The data occur from sunset to 5 h after sunset, and data with rain ($R_{sum} > 0.3$ mm) and fog (relative humidity > 80%) have been excluded.

increases from 0.024 to 0.042 K (from ~2 to ~3%) and remains very small.

The quantification of a_1 results in the following diagnostic equation for the daily maximum UHI:

$$UHI_{max} = \left(2 - SVF - f_{veg}\right) \sqrt[4]{\frac{S^{\downarrow} DTR^3}{U}} \qquad (13)$$

This formula is derived and therefore valid for $0 < f_{veg} < 0.4$ and $0.2 < SVF < 0.9$. Note that in the limit of f_{veg} and SVF going to 1, a_1 is zero and the UHI_{max} will vanish, as can be physically expected. U is limited to values higher than 0.5 ms^{-1}, however the cup anemometers used in the Dutch rural stations are unreliable with wind speeds lower than 1 ms^{-1}.

Figure 7 shows the performance of Equation (13) for the validation data set of each city in Table 1. Generally, the new equation performs reasonably well given its simplicity, with an RMSE of 0.91 K and a MEAE of only 0.58 K.

7. Discussion

In this study, a new diagnostic equation to estimate the UHI_{max} has been presented. Here, we discuss the main observational and methodological uncertainties and we will synthesize the current findings in the literature.

There have been previous attempts to scale the UHI using a simple equation. Summers (1964) suggested using the atmospheric boundary-layer height and the potential temperature gradient above the boundary layer to estimate the UHI in Montreal, Canada (Oke and East, 1971). However, the application of such an equation is difficult because vertical profiles are not routinely measured in most parts of the world, and where available are typically limited to once or twice a day.

Hidalgo *et al.* (2010) proposed to use the difference in the sensible heat flux between the rural and urban surface and the boundary-layer height to scale the UHI using numerical experiments. From an observational perspective, both boundary-layer height and surface heat fluxes are not routinely measured at WMO weather stations. Furthermore, energy balance measurements have additional issues dependent on the measurement technique and the instrument's footprint. Similarly, Lee *et al.* (2014) estimated the time-dependent UHI with the difference in sensible heat flux, the wind and a length scale of the city. Note that none of these studies use any urban morphology parameters, such as a measure for vegetation cover, building density or materials, whereas the current study does. Moreover, the diagnostic equation derived here only uses routine meteorological measurements, such as 10-m wind speed, solar radiation and 1.5-m temperature.

Alternatively, Oke (1998) and Runnalls and Oke (2000) developed a model for the diurnal cycle of the UHI. Their model is based on a weather factor depending on cloud fraction and cloud type, and the wind speed to the power of − 1/2. However, our results indicate that a dependence of UHI_{max} to the wind speed with a power of − 1/2 does not correspond to the current observations (Figure 5(c)). In that case, the model overestimates UHI_{max} for low UHI_{max} values, and underestimates UHI_{max} for high UHI_{max} values. Note that Oke (1998) formulated their model based on observations from North American cities, whereas here we explored European data. Hence, the relation between wind speed and the UHI_{max} might vary for example between

regions, climate zones, land use and roughness. In addition, their model also requires information on the observed cloud types, a parameter that is not routinely observed (nowadays).

In this study, we have utilized weather stations set-up by hobby meteorologists that are located in gardens, and rooftop stations have been eliminated. Unfortunately, this gives a limited variability in urban climate zones where measurements are taken (Table 1). The urban stations in Paris, Amsterdam and Köln gave much more information about including surface morphological properties into Equation (13). It is also important to note that the sky-view factor not only indicates the street geometry but also the building density and the location within the city, on the edge or in the centre, because the building density is generally higher in the centre of a large city.

In this study, our diagnostic equation has solely been derived from observations originating from northwestern Europe. This region of the world does not have many high-rise buildings (as in North-America or Asia) and has buildings with similar thermal properties. In addition, the variety in the climate within the utilized data sets is rather limited. All stations are located in a mild maritime climate (Cfb), with relatively cool summers and mild winters, where evaporation is usually not limited by soil moisture availability. Hence, we observe a large range of weather types and therefore a broad range in $UHI_{\max}$ magnitudes.

Note that this diagnostic equation does not account for several other urban properties such as building materials, anthropogenic heat and water fraction. This research assumed that building properties are generally similar, which is not unreasonable to assume in Western Europe. Applying the equation to areas with different ways of building houses and offices in for example Asia or North-America, other urban properties may need to be included in a_1 (Equation (12)). Here, we could think of variables such as thermal admittance, soil moisture and albedo. For example, it may be more accurate to use the impervious surface fraction because bare soil also evaporates. This would make the equation more applicable in other climates where bare soil is more common. However, in this case, we choose the vegetation fraction because it is more easily derivable using satellite images (e.g. green fraction, normalized difference vegetation index (NDVI)) available to the public. Defining the impervious surface fraction requires a more complex approach (e.g. Wu, 2004). In addition, Figure (5) shows that the vegetation fraction is sufficiently correlated to the $UHI_{\max}$. Similarly, anthropogenic heat is not included in Equation (13). Therefore, the equation should not be applied in places with heavy industry, and in the mid- or high-latitude winter season when anthropogenic heating is large. However, if the amount of anthropogenic heat release is known, it could be added to $S^{\downarrow}$ or added as a new variable in the dimensional analysis. This was not attempted in this research due to the uncertainty in the available methods of estimating anthropogenic heat. Concerning the water fraction, water dampens the diurnal temperature range inside and outside the city. The DTR of the rural area will be influenced by the proximity to the sea or other large water body. Therefore, the diagnostic equation performs best when the city and the rural station are of approximately similar distance to a water body. Equation (13) is not influenced by small channels, lakes or ponds within the city.

Above we mainly discussed the urban surface properties that can influence the $UHI_{\max}$. In addition, we only examined measurements above grass and cropland as rural reference sites and did not test the performance above contrasting rural land surface types. However, a rural location with a bare soil, a forest or an extreme amount of soil moisture availability will influence the cooling ability of the rural environment. The rural cooling effect is implicitly included in the DTR (Dai *et al.*, 1999; Bonan, 2001; De Wekker and Whiteman, 2006). For example, the cooling ability of a forest is generally less than dry, bare soil and the DTR will be smaller. Consequently, the $UHI_{\max}$ of a city with a forest surrounding it will have a smaller $UHI_{\max}$ compared to a city surrounded by dry, bare soil. However, a situation when the DTR will not sufficiently represents the urban *versus* rural cooling in the equation is snow cover, that is or is partially removed in the city. This can cause very large differences in urban temperatures (e.g. Klysik and Fortuniak, 1999)

Concerning the measured wind speed above the rural surface, the surface roughness and the measurement height influence the magnitude of the wind speed. In order to correct for the roughness of the rural terrain and the measurement height, the potential wind speed (U_p) can be used (Wieringa, 1986). For a measurement height of 10 m with low vegetation (a roughness length of about 0.03 m), the correction factor is 1, therefore the measured wind speed is the same as the potential wind speed. However, if the wind speed is measured at a location with a higher roughness length, the potential wind speed increases.

While using the dimensional analysis method to derive an equation for $UHI_{\max}$, there was not a sufficient number of variables to create completely independent groups. While deriving Equation (13), both dimensionless groups included *DTR*. This means that there may be some degree of self-correlation between Π_1 and Π_2 in Figure (3). In order to determine the amount of self-correlation, Baas *et al.* (2006) proposed randomizing all of the individual variables of the observational data set. Randomizing the data set used in this research and redrawing Figure (3) showed very scattered results without any obvious relation. This gives us confidence that self-correlation does not characterize the relation between the two dimensionless groups.

8. Conclusions

In this study, a diagnostic equation was derived to estimate the daily maximum UHI within the urban canyon. Key meteorological variables obtained from routine rural

weather station data, solar radiation, diurnal temperature range, wind speed and the vertical temperature gradient, and their relation to the UHI were analysed. Using these variables, multiple equations for the UHI could be composed and evaluated. Equation (13) performed best after including the most relevant urban morphology parameters (in this case, sky-view factor and vegetation fraction) for several cities in northwestern Europe.

The diagnostic Equation (13) is relatively simple, physically based and is in good agreement with field observations. It only requires routine observations or forecasts of screen-level temperature, solar radiation and 10-m wind speed in the rural area. However, the variety of cities tested is limited and further evaluation of cities outside northwestern Europe is needed.

The analytical equation is straightforward to apply in practice and gives a surprisingly satisfactory estimation of the daily maximum UHI under different weather conditions, without running a complicated and time-consuming urban canopy or atmospheric numerical model. This equation for the nocturnal canopy UHI allows for applications far beyond urban meteorological or climate studies. Amongst others, applications might include energy demand and health studies, requiring a representation of the night-time thermal environment of cities.

Acknowledgements

The authors thank Bert Heusinkveld for setting up and maintaining the measurement networks in Amsterdam and Wageningen, the KNMI and the UK Met Office for their measurement data sets. We thank Pierre Cellier, Benjamin Loubet and Nicolas Mascher from INRA Grignon for the Grignon (France) data set, Marius Schmidt, Alexander Graf, Daniel Weymann and Heye Bogena from Forschungszentrum Jülich for the Selhausen Jülich data set and the hobby meteorologists for providing their data sets that made this possible. Duick Thomas Young prepared the Birmingham data set. HiTemp (high-resolution temperature measurements within the urban environment) data are used with permission from the Birmingham Urban Climate Laboratory (BUCL), University of Birmingham, United Kingdom (http://www.bucl.org.uk/). HiTemp was funded by the Natural Environment Research Council (NERC) 'Network of Sensors' call (grants NE/I006915/1 and NE/I007032/1). This research was funded by NWO project CESAR as part of the program 'Sustainable accessibility to the Randstad' (grant 434.09.012), NWO – eScience project 'Summer in the City' (grant 027.012.103) and NWO – eScience project 'ERA-URBAN' (grant 027.014.203)

Appendix:

Here, the derivation for the dimensionless groups Π_1 and Π_2 is shown. We start with the following equation:

$$\Pi = UHI_{\max}^{\alpha} S^{\downarrow\beta} DTR^{\gamma} U^{\delta} \tag{A1}$$

Here, α, β, γ and δ are the exponents for each variable. Based on the number of dimensions, i.e. three in this case, we obtain the following system of equations:

$$\begin{cases} \alpha + \beta + \gamma = 0 \\ \beta + \delta = 0 \\ -\beta - \delta = 0 \end{cases}$$

where we see that the last two equations are equal and including both equations does not provide any additional information. Therefore, we can create two dimensionless groups. In order to create these dimensionless groups, we chose two parameters. For the first group, we choose $\beta = 0$ and $\delta = 0$:

$$\begin{cases} \alpha + 0 + \gamma = 0 \\ 0 + 0 = 0 \\ -0 - 0 = 0 \end{cases}$$

Consequently, $\alpha = 1$ and $\gamma = -1$ resulting in $\Pi_1 = UHI_{\max}^{1} S^{\downarrow 0} DTR^{-1} U^{0}$ giving:

$$\Pi_1 = \frac{UHI_{\max}}{DTR} \tag{A2}$$

For the second group, we choose $\alpha = 0$ and $\delta = -1$:

$$\begin{cases} 0 + \beta + \gamma = 0 \\ \beta - 1 = 0 \\ -\beta + 1 = 0 \end{cases}$$

Consequently, $\beta = 1$ and $\gamma = -1$ resulting in $\Pi_2 = UHI_{\max}^{0} S^{\downarrow 1} DTR^{-1} U^{-1}$ giving:

$$\Pi_2 = \frac{S^{\downarrow}}{U \cdot DTR} \tag{A3}$$

References

Ackerman B. 1985. Temporal march of the Chicago heat island. *J. Clim. Appl. Meteorol.* **24**(6): 547–554.

Arnfield AJ. 2003. Two decades of urban climate research: a review of turbulence, exchanges of energy and water, and the urban heat island. *Int. J. Climatol.* **23**(1): 1–26.

Baas P, Steeneveld G, Van De Wiel B, Holtslag A. 2006. Exploring self-correlation in flux-gradient relationships for stably stratified conditions. *J. Atmos. Sci.* **63**(11): 3045–3054.

Baik JJ, Kim YH, Kim JJ, Han JY. 2007. Effects of boundary-layer stability on urban heat island-induced circulation. *Theor. Appl. Climatol.* **89**(1–2): 73–81.

Bell S, Cornford D, Bastin L. 2015. How good are citizen weather stations? Addressing a biased opinion. *Weather* **70**(3): 75–84.

Blackadar AK. 1962. Exchange in a neutral atmosphere. *J. Geophys. Res.* **67**(8): 3095–3102.

Bonan GB. 2001. Observational evidence for reduction of daily maximum temperature by croplands in the Midwest United States. *J. Clim.* **14**(11): 2430–2442.

Bottyán Z, Unger J. 2003. A multiple linear statistical model for estimating the mean maximum urban heat island. *Theor. Appl. Climatol.* **75**(3–4): 233–243.

Buckingham E. 1914. On physically similar systems; illustrations of the use of dimensional equations. *Phys. Rev.* **4**: 345–376.

Businger JA, Wyngaard JC, Izumi Y, Bradley EF. 1971. Flux-profile relationships in the atmospheric surface layer. *J. Atmos. Sci.* **28**(2): 181–189.

Chapman L, Muller CL, Young DT, Warren EL, Grimmond CSB, Cai XM, Ferranti EJ. 2015. The Birmingham Urban Climate Laboratory: an open meteorological testbed and challenges of the smart city. *Bull. Am. Meteorol. Soc.* **96**(9): 1545–1560.

Chen F, Kusaka H, Bornstein R, Ching J, Grimmond CSB, Grossman-Clarke S, Loridan T, Manning KW, Martilli A, Miao S, Sailor D, Salamanca FP, Taha H, Tewari M, Wang X, Wyszogrodzki AA, Zhang C. 2011. The integrated WRF/urban modelling system: development, evaluation, and applications to urban environmental problems. *Int. J. Climatol.* **31**(2): 273–288.

Dai A, Trenberth KE, Karl TR. 1999. Effects of clouds, soil moisture, precipitation, and water vapor on diurnal temperature range. *J. Clim.* **12**(8): 2451–2473.

De Wekker SF, Whiteman CD. 2006. On the time scale of nocturnal boundary layer cooling in valleys and basins and over plains. *J. Appl. Meteorol. Climatol.* **45**(6): 813–820.

Delage Y. 1974. A numerical study of the nocturnal atmospheric boundary layer. *Q. J. R. Meteorol. Soc.* **100**(425): 351–364.

Dimoudi A, Nikolopoulou M. 2003. Vegetation in the urban environment: microclimatic analysis and benefits. *Energy Buildings* **35**(1): 69–76 (Special issue on urban research).

Dyer A. 1974. A review of flux-profile relationships. *Bound.-Layer Meteorol.* **7**(3): 363–372.

Eliasson I. 1996. Urban nocturnal temperatures, street geometry and land use. *Atmos. Environ.* **30**(3): 379–392.

Fortuniak K, Klysik K, Wibig J. 2006. Urban–rural contrasts of meteorological parameters in Lódz. *Theor. Appl. Climatol.* **84**(1–3): 91–101.

Gallo KP, Easterling DR, Peterson TC. 1996. The influence of land use/land cover on climatological values of the diurnal temperature range. *J. Clim.* **9**(11): 2941–2944.

Hidalgo J, Masson V, Gimeno L. 2010. Scaling the daytime urban heat island and urban-breeze circulation. *J. Appl. Meteorol. Climatol.* **49**(5): 889–901.

Hoffmann P, Krueger O, Schlünzen KH. 2012. A statistical model for the urban heat island and its application to a climate change scenario. *Int. J. Climatol.* **32**(8): 1238–1248.

Holmer B, Thorsson S, Lindén J. 2013. Evening evapotranspirative cooling in relation to vegetation and urban geometry in the city of Ouagadougou, Burkina Faso. *Int. J. Climatol.* **33**(15): 3089–3105.

Hu XM, Klein PM, Xue M, Lundquist JK, Zhang F, Qi Y. 2013. Impact of low-level jets on the nocturnal urban heat island intensity in Oklahoma City. *J. Appl. Meteorol. Climatol.* **52**(8): 1779–1802.

Kidder SQ, Essenwanger OM. 1995. The effect of clouds and wind on the difference in nocturnal cooling rates between urban and rural areas. *J. Appl. Meteorol.* **34**(11): 2440–2448.

Klysik K, Fortuniak K. 1999. Temporal and spatial characteristics of the urban heat island of Łódź, Poland. *Atmos. Environ.* **33**(24): 3885–3895.

Kusaka H, Chen F, Tewari M, Dudhia J, Gill DO, Duda MG, Wang W, Miya Y. 2012. Numerical simulation of urban heat island effect by the WRF model with 4-km grid increment: an inter-comparison study between the urban canopy model and slab model. *J. Meteorol. Soc. Jpn.* **90**(0): 33–45.

Langhaar HL. 1951. *Dimensional Analysis and Theory of Models*, Vol. **2**. Wiley: New York, NY.

Lee D. 1979. The influence of atmospheric stability and the urban heat island on urban-rural wind speed differences. *Atmos. Environ.* **13**(8): 1175–1180.

Lee TW, Choi HS, Lee J. 2014. Generalized scaling of urban heat island effect and its applications for energy consumption and renewable energy. *Adv. Meteorol.* **2014**: 5.

Lehuger S, Gabrielle B, Cellier P, Loubet B, Roche R, Béziat P, Ceschia E, Wattenbach M. 2010. Predicting the net carbon exchanges of crop rotations in Europe with an agro-ecosystem model. *Agric. Ecosyst. Environ.* **139**: 384–395.

Marciotto E, Oliveira A, Hanna S. 2010. Modeling study of the aspect ratio influence on urban canopy energy fluxes with a modified wall-canyon energy budget scheme. *Build. Environ.* **45**(11): 2497–2505.

Morris C, Simmonds I, Plummer N. 2001. Quantification of the influences of wind and cloud on the nocturnal urban heat island of a large city. *J. Appl. Meteorol.* **40**(2): 169–182.

Oke T, East C. 1971. The urban boundary layer in Montreal. *Bound.-Layer Meteorol.* **1**(4): 411–437.

Oke TR. 1981. Canyon geometry and the nocturnal urban heat island: comparison of scale model and field observations. *J. Climatol.* **1**(3): 237–254.

Oke TR. 1982. The energetic basis of the urban heat island. *Q. J. R. Meteorol. Soc.* **108**(455): 1–24.

Oke TR. 1998. An algorithmic scheme to estimate hourly heat island magnitude. In *Proceedings of 2nd* Symposium *Urban* environment, 80–83.

Park HS. 1986. Features of the heat island in Seoul and its surrounding cities. *Atmos. Environ.* **20**(10): 1859–1866.

Petralli M, Massetti L, Brandani G, Orlandini S. 2014. Urban planning indicators: useful tools to measure the effect of urbanization and vegetation on summer air temperatures. *Int. J. Climatol.* **34**(4): 1236–1244.

Runnalls K, Oke T. 2000. Dynamics and controls of the near-surface heat island of Vancouver, British Columbia. *Phys. Geogr.* **21**(4): 283–304.

Salamanca F, Martilli A, Tewari M, Chen F. 2011. A study of the urban boundary layer using different urban parameterizations and high-resolution urban canopy parameters with WRF. *J. Appl. Meteorol. Climatol.* **50**(5): 1107–1128.

Steeneveld G, Van de Wiel B, Holtslag A. 2006. Modeling the evolution of the atmospheric boundary layer coupled to the land surface for three contrasting nights in CASES-99. *J. Atmos. Sci.* **63**(3): 920–935.

Steeneveld GJ, Koopmans S, Heusinkveld BG, van Hove LWA, Holtslag AAM. 2011. Quantifying urban heat island effects and human comfort for cities of variable size and urban morphology in the Netherlands. *J. Geophys. Res.* **116**(D20).

Steeneveld GJ, Van de Wiel BJH, Holtslag AAM. 2007. Diagnostic equations for the stable boundary layer height: evaluation and dimensional analysis. *J. Appl. Meteorol. Climatol.* **46**(2): 212–225.

Stewart ID, Oke TR. 2012. Local climate zones for urban temperature studies. *Bull. Am. Meteorol. Soc.* **93**(12): 1879–1900.

Summers P. 1964. *A Urban Ventilation Model Applied to Montreal*. PhD thesis, McGill University, Canada.

Szymanowski M, Kryza M. 2012. Local regression models for spatial interpolation of urban heat island – an example from Wroc$_{l}$aw, SW Poland. *Theor. Appl. Climatol.* **108**(1–2): 53–71.

Theeuwes NE, Steeneveld GJ, Ronda RJ, Heusinkveld BG, van Hove LWA, Holtslag AAM. 2014. Seasonal dependence of the urban heat island on the street canyon aspect ratio. *Q. J. R. Meteorol. Soc.* **140**(684): 2197–2210.

Theeuwes NE, Steeneveld GJ, Ronda RJ, Rotach MW, Holtslag AAM. 2015. Cool city mornings by urban heat. *Environ. Res. Lett.* **10**(11): 114022.

Wieringa J. 1986. Roughness-dependent geographical interpolation of surface wind speed averages. *Q. J. R. Meteorol. Soc.* **112**(473): 867–889.

Wolters D, Brandsma T. 2012. Estimating the urban heat island in residential areas in the Netherlands using observations by weather amateurs. *J. Appl. Meteorol. Climatol.* **51**(4): 711–721.

Wu C. 2004. Normalized spectral mixture analysis for monitoring urban composition using ETM+ imagery. *Remote Sens. Environ.* **93**(4): 480–492.

